Assessment of Thermal Instabilities and Oscillations in Multifinger Heterojunction Bipolar Transistors Through a Harmonic-Balance-Based CAD-Oriented Dynamic Stability Analysis Technique

Fabio Lorenzo Traversa, Federica Cappelluti, *Member, IEEE*, Fabrizio Bonani, *Senior Member, IEEE*, and Giovanni Ghione, *Fellow, IEEE*

***Abstract*—We present a novel analysis of thermal instabilities and oscillations in multifinger heterojunction bipolar transistors (HBTs), based on a harmonic-balance computer-aided-design (CAD)-oriented approach to the dynamic stability assessment. The stability analysis is carried out in time-periodic dynamic conditions by calculating the Floquet multipliers of the limit cycle representing the HBT working point. Such a computation is performed directly in the frequency domain, on the basis of the Jacobian of the harmonic-balance problem yielding the limit cycle. The corresponding stability assessment is rigorous, and the efficient calculation method makes it readily implementable in CAD tools, thus allowing for circuit and device optimization. Results on three- and four-finger layouts are presented, including closed-form oscillation criteria for two-finger devices.**

***Index Terms*—Electrothermal effects, heterojunction bipolar transistors (HBTs), stability.**

I. Introduction

THE ANALYSIS of electrothermal instabilities in semiconductor devices is a classical problem, which has been the object of discussion for decades (see [1] and [2] and the references therein), above all with reference to bipolar transistors. In particular, the development of stabilization strategies for heterojunction bipolar transistors (HBTs) through thermal or electrical approaches (such as thermal shunting or emitter ballasting) on the basis of approximate thermal models and of a dc stability assessment has been the object of extensive investigation (see, e.g., [3] and [4]).

In this paper, we revisit the electrothermal stability problem through a general and rigorous approach for stability analysis in large-signal dynamic conditions, namely, the Floquet multiplier theory [5]. The proposed implementation, based on the harmonic-balance technique for large-signal (quasi)-periodic steady-state evaluation, is readily amenable to inclusion in computer-aided design (CAD) tools for circuit analysis and can be exploited to address more general stability problems than the one presently considered, like the large-signal stability analysis of power amplifiers, or the design of oscillators.

The present approach, briefly discussed in Section II, allows one to study the stability of the solution of a nonlinear dynamical system, assuming that the latter is a periodic function of time (i.e., a limit cycle [5]). In this case, the stability analysis corresponds to assessing the stability of the limit cycle with respect to an external perturbation, which we carry out by evaluating the Floquet multipliers [5] of the limit cycle itself. According to the algorithm presented in [6], such an evaluation is performed directly in the frequency domain, making use of the popular harmonic-balance approach. This is a significant advantage over the time-domain calculation of the Floquet multipliers, often exploited in the more mathematically oriented literature, because no cumbersome numerical time integration of the linearized system is required.

The general methodology is used here to study the gain collapse phenomenon in GaAs-based HBTs. We have previously reported on the analysis of electrothermal induced instability in GaAs-based HBTs under large-signal and pulsed operation [7]. In this paper, we exploit the proposed Floquet-multiplier-based technique to show an extremely varied set of dynamical behaviors, for instance, *versus* the device layout (namely, the number of emitter fingers). A further advantage of the present approach is the possibility to accurately and efficiently assess the effect of electrical or thermal stabilization techniques [8]. Two main additions are presented here with respect to [8]. First, we add an introduction to the stability analysis technique in order to make this paper self-consistent and allow the reader to have a better insight into the implementation. Furthermore, we provide insights into the appearance of electrothermal oscillations, which were reported for multifinger device layouts in [8]. A detailed numerical analysis of the dynamic behavior of a two-finger device is added, and the onset of the oscillations is explained on the basis of a more intuitive electrothermal circuit model. This allows one to obtain an analytical set of stability and oscillation conditions.

Manuscript received May 11, 2009; revised July 20, 2009. First published October 30, 2009; current version published December 09, 2009. This work was supported by Project CNT4SIC, funded by Regione Piemonte under Bando regionale sulla ricerca industriale e lo sviluppo precompetitivo per l'anno 2006.

F. L. Traversa was with the Dipartimento di Elettronica, Politecnico di Torino, Turin 10129, Italy. He is now with the Departament d'Enginyeria Electrònica, Universitat Autònoma de Barcelona, Barcelona 08193, Spain (e-mail: fabiolorenzo.traversa@uab.cat).

F. Cappelluti, F. Bonani, and G. Ghione are with the Dipartimento di Elettronica, Politecnico di Torino, Turin 10129, Italy (e-mail: federica.cappelluti@polito.it; fabrizio.bonani@polito.it; giovanni.ghione@polito.it).

Color versions of one or more of the figures in this paper are available online at http://ieeexplore.ieee.org.

Digital Object Identifier 10.1109/TMTT.2009.2034229

II. Harmonic-Balance-Based Stability Analysis Approach

The Floquet theory is a classical topic in the perturbation analysis of nonlinear dynamical systems with a finite number of states and can be considered as the fundamental tool for stability analysis of time-periodic solutions. Originally devised for nonlinear systems expressed in terms of ordinary differential equations, it has recently been extended [9] to the case of differential-algebraic equations. The extension is practically relevant to the analysis of lumped circuits, whose describing equations are of differential-algebraic type; on the other hand, the main limitation of the method lies on the fact that distributed elements cannot be represented in such a form.

A. Survey of Floquet Stability Theory

For the sake of simplicity, we shall review in this section the Floquet analysis in the case of a 1-D differential-algebraic equation, i.e., a nonlinear dynamical system represented by $n = 1$ state variables. This will allow one to introduce the proposed numerical approach in a simple way; the general (vector) case is treated in detail in [6]. Let us consider the following nonlinear scalar differential-algebraic equation, which has the typical form resulting from the application of the modified nodal analysis to a lumped circuit [10]:

$$\frac{\mathrm{d}}{\mathrm{d}t}q\left(x(t)\right) + g\left(x(t)\right) = s(t) \tag{1}$$

where $x(t)$ is the (real) state variable of the system, $s(t)$ is the applied forcing term, and $q(\cdot)$ and $g(\cdot)$ are two nonlinear functions of $x(t)$ regular enough to ensure that if a periodic solution of (1) exists, it can be developed in Fourier expansion. We consider here the case of a time-periodic excitation $s(t) = s(t+T)$, where T is the period, assuming that a T-periodic solution $x_S(t) = x_S(t+T)$ (the *steady state* of the circuit) satisfies (1). $x_S(t)$ is also called a *limit cycle* for (1). Notice that the following perturbation theory holds also for autonomous systems (like free-running oscillators), where $s(t) = 0$, under the assumption that a nontrivial T-periodic solution is present.

The stability properties of the limit cycle are assessed by performing a perturbation analysis of the differential–algebraic equation around the steady-state solution, i.e., by linearizing (1) around $x_S(t)$

$$\frac{\mathrm{d}}{\mathrm{d}t}\left[C(t)z(t)\right] + A(t)z(t) = 0 \tag{2}$$

where $C(t)$ and $A(t)$ are two T-periodic functions corresponding to the first derivative[1] of $q(x)$ and $g(x)$ calculated in $x_S(t)$

$$C(t) = \left.\frac{\mathrm{d}q}{\mathrm{d}x}\right|_{x_S(t)} \qquad A(t) = \left.\frac{\mathrm{d}g}{\mathrm{d}x}\right|_{x_S(t)}. \tag{3}$$

According to [9], the solution of (2) takes the form

$$z(t) = e^{\mu t}u(t) \tag{4}$$

where $u(t)$ is a T-periodic function and μ is called the Floquet exponent of the limit cycle $x_S(t)$. The associated Floquet multiplier is defined as $\lambda = \exp(\mu T)$. Substituting (4) into (2) yields an equation involving, as unknowns, both μ and $u(t)$

$$\frac{\mathrm{d}}{\mathrm{d}t}\left[C(t)u(t)\right] + \mu C(t)u(t) + A(t)u(t) = 0. \tag{5}$$

In the general n-dimensional case, there are n independent Floquet exponents and, correspondingly, n Floquet multipliers [9]. Notice that, for $n > 1$, the Floquet exponents can either be real or complex, but in the latter case, they have to appear in complex conjugate pairs to ensure that $z(t)$ is real. Clearly, (asymptotic) stability is assured only if all the Floquet exponents have a negative real part,[2] i.e., if all of the Floquet multipliers are located inside the unit circle in the complex plane. According to [11], when one of the Floquet multipliers crosses the unit circle, the limit cycle undergoes a bifurcation. The $\lambda = +1$ case corresponds to a fold bifurcation, and $\lambda = -1$ is a flip (or period-doubling) bifurcation, while if λ is complex, the bifurcation is of Neimark–Sacker type. Notice that, for Neimark-Sacker bifurcations, two Floquet multipliers always undergo the unit circle crossing; furthermore, the presence of a non-null imaginary part gives rise to amplitude oscillations in the solution [see (4)].

B. Harmonic-Balance Evaluation of the Floquet Multipliers

Harmonic balance is a popular numerical technique for the direct frequency-domain evaluation of the steady-state solution of nonlinear dynamic equations admitting a limit cycle [12]. Harmonic balance is available in the vast majority of circuit simulators used for RF/microwave design. The numerical algorithm briefly discussed here (the full description can be found in [6]) is readily implementable into any harmonic-balance simulator.

According to the harmonic-balance approach [12], each real T-periodic function $\alpha(t)$ is represented through a (truncated) Fourier series

$$\alpha(t) = \sum_{h=0}^{N_H} \alpha_h(t) \tag{6a}$$

$$\alpha_h(t) = \begin{cases} \tilde{\alpha}_{\mathrm{c}0}, & h = 0 \\ \tilde{\alpha}_{\mathrm{c}h}\cos(h\omega t) + \tilde{\alpha}_{\mathrm{s}h}\sin(h\omega t), & h \neq 0 \end{cases} \tag{6b}$$

and the period $]0, T]$ is sampled into $2N_H + 1$ time samples t_h. This allows one to define the vector of the time samples

$$\boldsymbol{\alpha} = \left[\alpha(t_1), \ldots, \alpha(t_{2N_H+1})\right]^{\mathrm{T}} \tag{7}$$

and the vector of the harmonic amplitudes

$$\tilde{\boldsymbol{\alpha}} = \left[\tilde{\alpha}_{\mathrm{c}0}, \tilde{\alpha}_{\mathrm{c}1}, \tilde{\alpha}_{\mathrm{s}1}, \ldots, \tilde{\alpha}_{\mathrm{c}N_H}, \tilde{\alpha}_{\mathrm{s}N_H}\right]^{\mathrm{T}}. \tag{8}$$

The two sampled representations of $\alpha(t)$ are related by an invertible linear operator (the discrete Fourier transform operator and its inverse [12])

$$\tilde{\boldsymbol{\alpha}} = \boldsymbol{\Gamma}\boldsymbol{\alpha} \Longleftrightarrow \boldsymbol{\alpha} = \boldsymbol{\Gamma}^{-1}\tilde{\boldsymbol{\alpha}} \tag{9}$$

[1] In the general n-dimensional case, the two functions are the Jacobian matrices of the two nonlinear vector functions appearing in (1). Notice that, in general, the Jacobian matrix $\mathbf{C}(t)$ may be not invertible.

[2] Apart from the case of oscillators, where one of the Floquet exponents is always zero, see [9].

whose detailed expression can be found in [6] and [12]. Similarly, the harmonic amplitudes of the time derivative (denoted here with a dot) of $\alpha(t)$ are linearly related to the harmonic amplitudes $\tilde{\boldsymbol{\alpha}}$ by means of a tridiagonal square matrix $\boldsymbol{\Omega}$ (see [6] for the expression)

$$\tilde{\dot{\boldsymbol{\alpha}}} = \boldsymbol{\Gamma}\dot{\boldsymbol{\alpha}} = \omega\boldsymbol{\Omega}\tilde{\boldsymbol{\alpha}} \tag{10}$$

where $\dot{\boldsymbol{\alpha}}$ denotes the collection of time samples of $\dot{\alpha}(t)$, and $\omega = 2\pi/T$.

Finally, we conclude these introductory remarks by considering the product of two T-periodic functions $\beta(t) = c(t)\alpha(t)$. The time samples of β are easily related to the time samples of α and c by means of

$$\boldsymbol{\beta} = \mathbf{c}\boldsymbol{\alpha} \tag{11}$$

where $\mathbf{c} = \mathrm{diag}\{c(t_h)\}$ is a diagonal matrix collecting the time samples of $c(t)$. Using (9), we find the harmonic amplitudes of $\beta(t)$ as

$$\tilde{\boldsymbol{\beta}} = \boldsymbol{\Gamma}\boldsymbol{\beta} = \boldsymbol{\Gamma}\mathbf{c}\boldsymbol{\Gamma}^{-1}\boldsymbol{\Gamma}\boldsymbol{\alpha} = \tilde{\mathbf{c}}\tilde{\boldsymbol{\alpha}} \tag{12}$$

where $\tilde{\mathbf{c}} = \boldsymbol{\Gamma}\mathbf{c}\boldsymbol{\Gamma}^{-1}$.

Using (9) –(12) into the time-sampled version of (5), we can derive the following relation linking the harmonic amplitudes of $u(t)$ and the Floquet exponent μ:

$$-(\tilde{\mathbf{A}} + \omega\boldsymbol{\Omega}\tilde{\mathbf{C}})\tilde{\boldsymbol{u}} = \mu\tilde{\mathbf{C}}\tilde{\boldsymbol{u}} \tag{13}$$

where $\tilde{\mathbf{A}}$ and $\tilde{\mathbf{C}}$ are the harmonic representations [compare with (12)] of $A(t)$ and $C(t)$, respectively. Notice that $\tilde{\mathbf{A}}$ and $\tilde{\mathbf{C}}$ are already available from the last step in the numerical procedure for the determination of $x_S(t)$ if the Newton method is exploited for the solution of the harmonic-balance problem.

Equation (13) is a generalized eigenvalue problem of size $2N_H + 1$; therefore, its solution yields $2N_H + 1$ values for μ. They are located in a vertical line in the complex plane (apart from numerical errors due to truncation) [6], where the difference between the imaginary parts of any two first neighboring values is $2\pi/T$. As discussed in [6], numerical considerations lead one to choose the value that is closer to the real axis as the better approximation of the actual Floquet exponent. In the general n-dimensional case, the size of (13) is $n(2N_H+1)$, and similar remarks on the placement of the eigenvalues in the complex plane hold.

III. Thermal Stability of Multifinger HBTs

The stability assessment technique described in Section II is applied to the study of the electrothermal behavior of multifinger GaAs-based HBTs [8]. The HBT electrical model exploits a measurement-based temperature-dependent Gummel–Poon model [13] for forward dc operation, completed by extrinsic resistances and nonlinear base–emitter and base-collector capacitances (see Fig. 1 for a comparison with experimental data), coupled to an RC thermal network extracted from 3-D thermal simulations, which describes self- and mutual-finger heating (see, e.g., [13]). For expediency, a simplified low-order thermal network has been exploited to minimize the number of state variables. The base current of each finger is expressed as

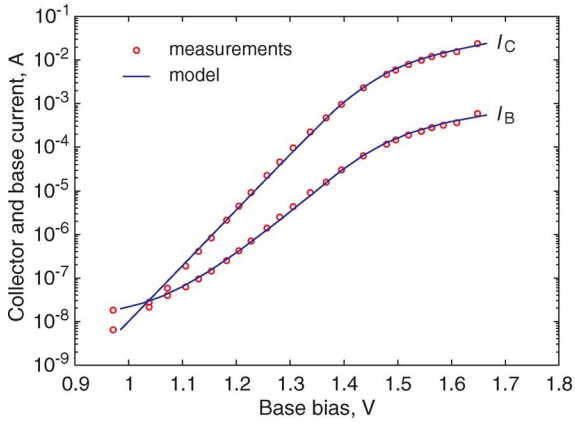

Fig. 1. Comparison between the measured and simulated HBT Gummel plots for a single-finger device (data from [13]).

$$i_{\mathrm{B}k} = \frac{I_{\mathrm{C0}}}{\beta_{\mathrm{F}k}(T_k)} e^{-E_{\mathrm{g}}(T_k)/(k_{\mathrm{B}}T_k)} \left[e^{v_{\mathrm{BE}k}/(\eta_{\mathrm{F}}k_{\mathrm{B}}T_k)} - 1\right] + I_{\mathrm{B0}}\left[e^{v_{\mathrm{BE}k}/(\eta_{\mathrm{E}}k_{\mathrm{B}}T_k)} - 1\right] \tag{14}$$

where k denotes the finger index, T_k is the finger temperature, E_{g} is the base material energy gap, η_{F} is the ideality factor of the base–emitter junction, $I_{\mathrm{C0}}\exp[-E_{\mathrm{g}}(T_k)/(k_{\mathrm{B}}T_k)]$ is the base-emitter reverse saturation current, η_{E} is the ideality factor for the parasitic base current, I_{B0} represents such parasitic current in reverse saturation, and $\beta_{\mathrm{F}k}(T_k) = \beta_0\exp[\Delta E_{\mathrm{v}}/k_{\mathrm{B}}T_k)]$ is the finger gain excluding the parasitic base current. ΔE_{v} is the valence-band discontinuity of the base-emitter junction. The extrinsic resistance values are $R_{\mathrm{C}} = 16\ \Omega$, $R_{\mathrm{E}} = 10.34\ \Omega$, and $R_{\mathrm{B}} = 45\ \Omega$.

The temperature rise of each finger $\Delta T_k = \sum_i \Delta T_{k,i}$ is decomposed into self-contribution and cross-contribution whose dynamic behavior is calculated according to

$$\frac{\mathrm{d}\Delta T_{k,i}}{\mathrm{d}t} = -\frac{1}{R_{\mathrm{th}k,i}C_{\mathrm{th}k,i}}\Delta T_{k,i} + \frac{p_i}{C_{\mathrm{th}k,i}} \tag{15}$$

where $\Delta T_{k,i}$ is the temperature rise of the kth finger due to the power p_i dissipated into the ith finger, and $R_{\mathrm{th}k,i}$ and $C_{\mathrm{th}k,i}$ represent the self-thermal resistance and capacitance if $k = i$ and the mutual ones if $k \neq i$, respectively. The layout considered is made up of parallel and equally spaced emitter fingers (each finger is $3 \times 15\ \mu\mathrm{m}^2$, and the finger spacing is 30 μm). The substrate is GaAs (120 μm thick), with self-thermal resistance being equal to 1600 K/W. For first neighboring fingers, the mutual thermal resistance amounts to 100 K/W, while $R_{\mathrm{th}k,i}$ linearly scales with the inverse of distance for non-neighboring fingers. The self-capacitance and mutual (first neighbors) thermal capacitance are equal to 99 pJ/K and 28 nJ/K, respectively. For non-neighboring fingers, the scaling is similar to the resistances'. The results presented in the following are calculated operating the device in small-signal conditions at a frequency of 1 MHz. Furthermore, we consider here the constant-base-current operation because, in this case, GaAs HBTs undergo the well-known current-collapse phenomenon. The dc bias is set by

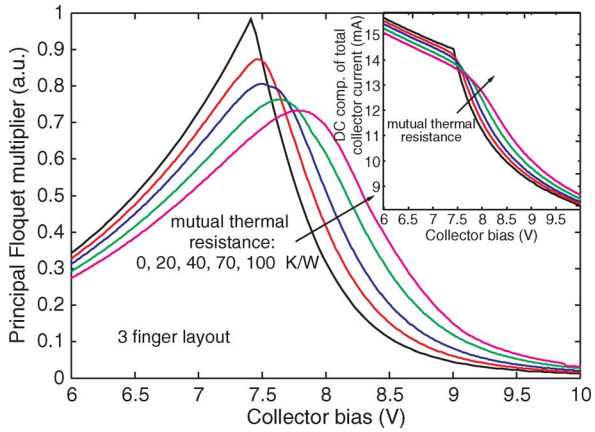

Fig. 2. Largest Floquet multiplier for the three-finger layout as a function of $V_{\rm CC}$ for different values of mutual thermal resistance ($I_{\rm Bt,0} = 0.6$ mA). The inset shows the corresponding dc output characteristics (data from [8]).

a total base current $I_{\rm Bt,0}$, which is divided among the $N_{\rm f}$ fingers of the layout.

A. Bifurcation Issue

The classical interpretation of current-gain collapse in HBTs [14] is based on the assumption that the uniform current solution that is valid in low-dissipation conditions undergoes a fold bifurcation as the dissipated power increases, so that one of the fingers becomes hotter than the other ones, thereby drawing all of the collector current and ultimately reducing the device current gain.

This is strictly true for $N_{\rm f} = 2$ (see the discussion hereinafter) but loses generality in the case of $N_{\rm f} > 2$, provided that thermal coupling between fingers is taken into account, as shown in Fig. 2, where the largest Floquet multiplier for the case of $N_{\rm f} = 3$ and for an increasing value of coupling thermal resistance is plotted as a function of the total collector bias $V_{\rm CC}$. The Floquet multiplier reaches $+1$ (i.e., a fold bifurcation) for no thermal coupling only, while in the presence of thermal coupling, the Floquet multiplier exhibits a maximum. Comparing the $V_{\rm CC}$ position of the maximum with the output dc curves (shown in the inset of Fig 2), the correlation between the two phenomena readily appears, thus justifying the use of the Floquet multiplier maximum as a probe to ascertain the onset of current-gain collapse. From a physical standpoint, the disappearance of bifurcation depends on the fact that, for $N_{\rm f} > 2$, the temperature distribution is nonuniform, even at low dissipated power (i.e., the central fingers are hotter than the lateral ones), thus preventing the uniform current solution to exist.

The dynamic behavior of two- and three-finger devices can be considered as the basis to understand what happens for a larger number of fingers because, for $N_{\rm f} > 3$, the instabilities are a combination of the instability patterns occurring in the elementary cases. For instance, let us consider $N_{\rm f} = 4$. As shown in the upper part of Fig. 3, the dc output characteristics exhibit two successive gain drops, whose physical interpretation can be obtained by observing the partial finger currents shown in the same photograph and comparing with the Floquet multipliers plotted in the lower part of Fig. 3. The first gain collapse corresponds to a maximum of the Floquet multiplier and to a first significant

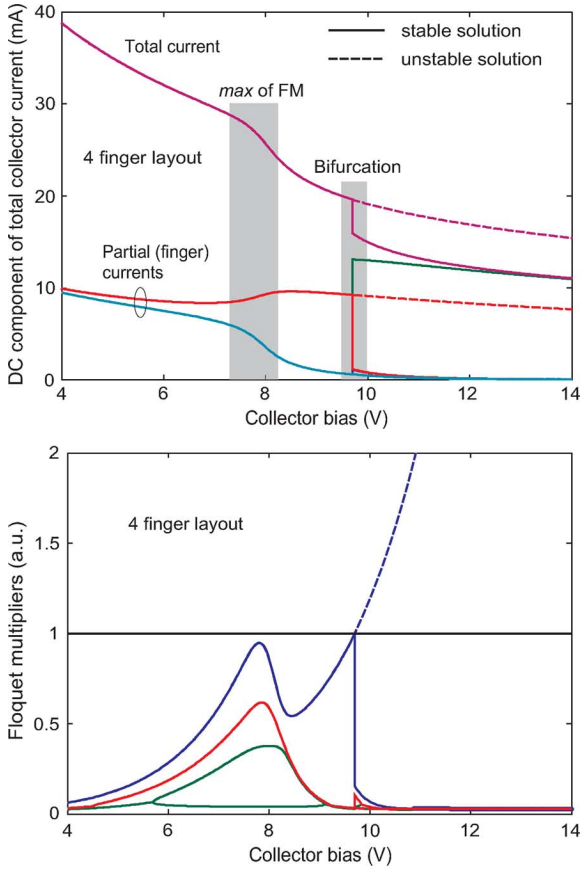

Fig. 3. (*top*) Total and partial dc components of collector currents for an $N_{\rm f} = 4$ and $I_{\rm Bt,0} = 1.8$ mA. (*bottom*) Floquet multipliers as a function of $V_{\rm CC}$. Data from [8].

difference between the currents drawn by the two inner and two outer fingers. Further increasing $V_{\rm CC}$, a fold bifurcation appears, in correspondence with a bifurcation between the currents in the two inner hotter device fingers (notice that the symmetrical solution becomes unstable).

B. Stabilization and Electrothermal Oscillations

From a technological standpoint, the mitigation of current-gain collapse is often attained by increasing the thermal coupling between the various fingers, thus contrasting (e.g., by introducing a thermal shunt air-bridge [16] in the device layout) the onset of a temperature imbalance among the fingers. This technique has some advantages with respect to using an electrical negative feedback, e.g., emitter or base ballasting resistances that, in turn, compromise the device gain. While the case of electrical feedback is treated in [8], we discuss here the effect on the electrothermal dynamics of the presence of a gold air-bridge. The air-bridge effect is approximated through a thermal conductance matrix coupled to the substrate thermal resistance matrix, while thermal capacitive effects associated to metallization are assumed negligible.

We consider first the case of $N_{\rm f} = 2$. Fig. 4 shows the $V_{\rm CC}$ dependence of the bifurcating Floquet multiplier for two different air-bridge thicknesses. For the thinner metal, and therefore for the lower thermal coupling between the fingers, the bifurcation is of fold type, as previously discussed (see also the

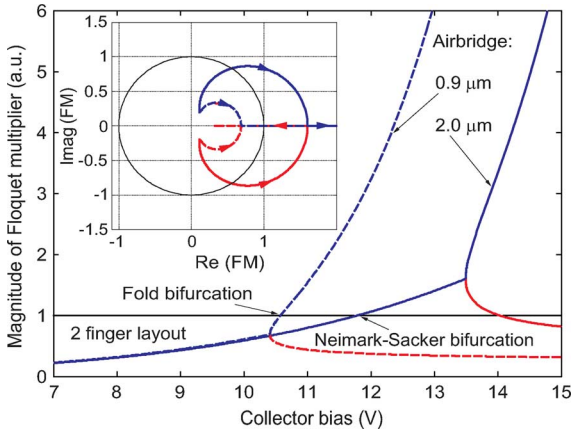

Fig. 4. Magnitude of the bifurcating Floquet multiplier (FM in the figure inset) as a function of $V_{\rm CC}$ for $N_{\rm f} = 2$. Two air-bridge thicknesses are considered.

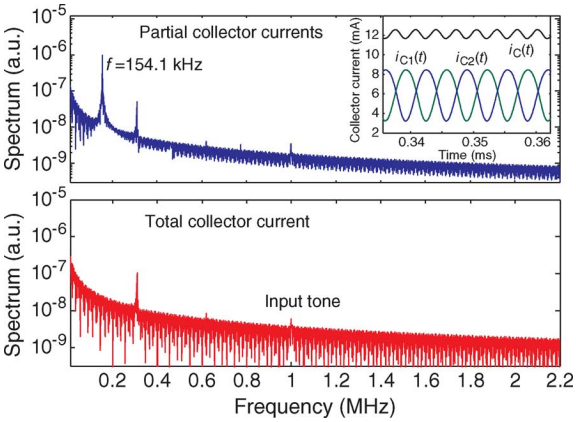

Fig. 5. Spectra of the partial and total collector currents for $N_{\rm f} = 2$. A 2-μm-thick air-bridge is considered, while $V_{\rm CC} = 11.9$ V, and the dc component of the total base current is 1 mA.

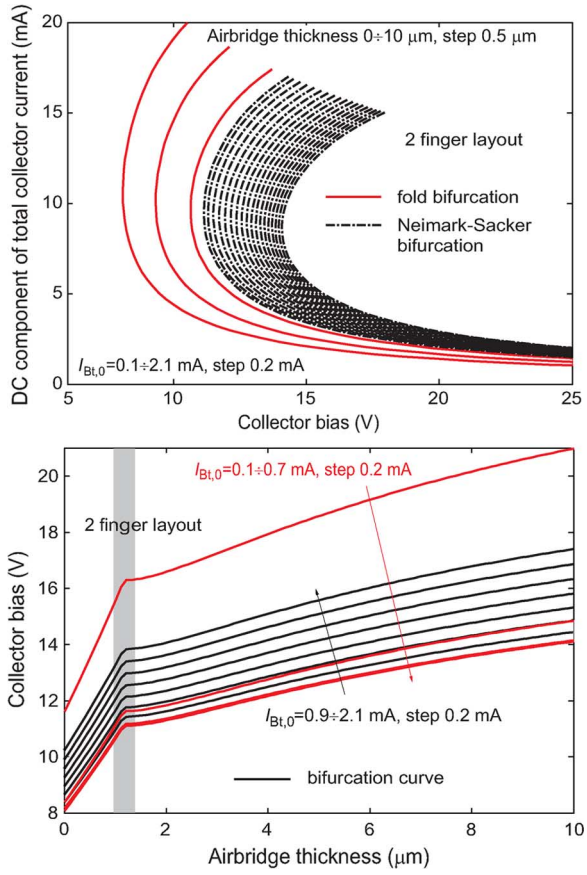

Fig. 6. Bifurcation curve in the (*top*) $(I_{\rm C}, V_{\rm CC})$ plane and (*bottom*) the ($V_{\rm CC}$, air-bridge thickness) plane for $N_{\rm f} = 2$. The shaded area shows the point where the bifurcation changes from fold to Neimark–Sacker type. Data from [15].

inset of Fig. 4, where the Floquet multiplier evolution in the complex plane is detailed). As the thermal coupling is increased, the dynamic behavior changes significantly because the bifurcation becomes of Neimark–Sacker type. This amounts to have two complex conjugate Floquet multipliers, with nonzero imaginary part, crossing the unit circle in the complex plane, and, therefore, to the presence of spurious oscillations. This is confirmed by time-domain simulations, which allow one to obtain the results shown in Fig. 5, where we show the spectra and the time-domain waveforms of the partial and total collector currents of the two-finger HBT with a thermal shunt thickness of 2 μm. The oscillation frequency predicted at the bifurcation onset ($V_{\rm CC} = 11.8$ V) is 156.3 kHz, and it slightly decreases as we move toward higher $V_{\rm CC}$ values. Notice that the frequency of the oscillations is totally uncorrelated from the small-signal input tone at 1 MHz. A detailed bifurcation analysis allows one to obtain the bifurcation curves shown in Fig. 6 as a function of air-bridge thickness, where it is shown how the dominant bifurcation becomes of Neimark–Sacker type for thermal coupling corresponding to an air-bridge thickness between 1 and 1.5 μm.

A similar behavior is evidenced for the case of $N_{\rm f} = 3$, as shown in Fig. 7. Of course, according to the discussion in Section III-A, for $N_{\rm f} > 2$, the gain collapse may also be due to a maximum in the Floquet multipliers. An interesting remark is that the onset of oscillations is moved toward larger thermal coupling, and this trend is also confirmed for $N_{\rm f} = 4$ [8].

C. Circuit Interpretation of Electrothermal Oscillations

Electrothermally induced low-frequency spurious oscillations were reported previously for bipolar devices [17], [18] and explained on the basis of an interplay between slow electrical dynamics (e.g., a bias-tee capacitance) external to the device and the device thermal memory. On the other hand, in the present case, oscillations are related to an energy exchange among the different fingers of the device, as discussed further on.

A simple physical interpretation of the oscillations is based on the linearized equivalent circuit of the self-consistent device model. In order to keep the derivation simple, and to be able to obtain closed-form results, we limit the discussion to the case of $N_{\rm f} = 2$. Furthermore, since the oscillation frequency lies well within the device bandwidth, we neglect here the electrical device memory effects (fully included in the complete model previously described), while we retain the reactive components associated to the thermal network.

The stability of the dc working point of the complete HBT electrothermal description is carried out through a linearization of the circuit around the dc equilibrium defined by ΔT_{Qk}, $I_{{\rm BQ}k}$ ($k = 1, 2$). The equivalent small-signal electrothermal circuit at

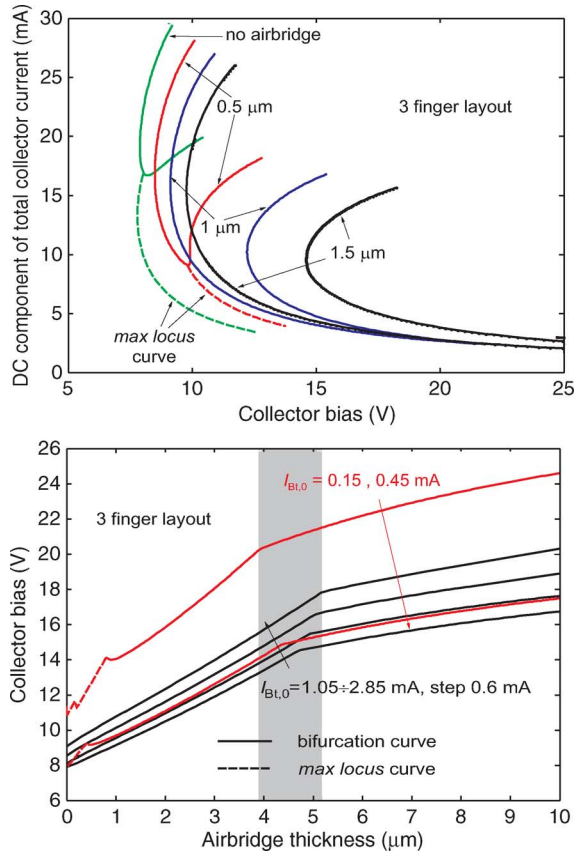

Fig. 7. Bifurcation curve in (*top*) the $(I_{\rm C}, V_{\rm CC})$ plane and in (*bottom*) the ($V_{\rm CC}$, air-bridge thickness) plane for $N_{\rm f} = 3$. The shaded area shows the point where the bifurcation changes from fold to Neimark–Sacker type. Data from [8].

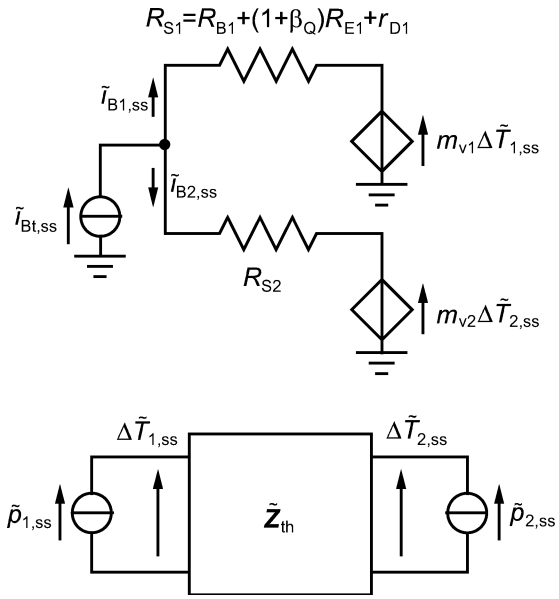

Fig. 8. Small-signal equivalent circuit of the base–emitter loop for a two-finger HBT coupled to the thermal circuit.

the base–emitter loop of the two-finger HBT is shown in Fig. 8, where

$$R_{Sk} = R_{{\rm B}k} + (1+\beta_{{\rm Q}k})R_{{\rm E}k} + r_{{\rm D}k} \tag{16}$$

is the conventional input resistance of a common–emitter stage because $r_{{\rm D}k} = (\partial v_{{\rm BE}k}/\partial i_{{\rm B}k})|_{I_{{\rm BQ}k},\Delta T_{{\rm Q}k}}$ is the base–emitter diode differential resistance. The thermal feedback is modeled through the temperature-controlled voltage source $m_{{\rm v}k}\Delta T_{k,{\rm ss}}$, where

$$m_{{\rm v}k} = m_{{\rm v}_{\rm BE}k} + R_{{\rm E}k} I_{{\rm BQ}k} m_{\beta k} \tag{17}$$

with $m_{{\rm v}_{\rm BE}k} = (\partial v_{{\rm BE}k}/\partial \Delta T_k)|_{I_{{\rm BQ}k},\Delta T_{{\rm Q}k}}$ and $m_{\beta k} = (\partial \beta_k/\partial \Delta T_k)|_{I_{{\rm BQ}k},\Delta T_{{\rm Q}k}}$. Since we addressed the stability analysis of the uniform collector-current solution, the working point and the corresponding small-signal parameters of the two fingers will be identical. For this reason, from now on, we will drop the finger subscript from such variables (notice, however, that $I_{\rm BQ} = I_{{\rm Bt},0}/2$ is the dc base-current value flowing in each finger, not the total one).

For the sake of simplicity, in the following derivation, the finger dissipated power is computed by neglecting the power dissipated at the base–emitter junction: $p_k \approx v_{{\rm CE}k} i_{{\rm C}k} = v_{{\rm CE}k}\beta(T_k) i_{{\rm B}k}$. Since we are dealing with a linearized equivalent circuit, we can operate in the frequency domain expressing the small-signal dissipated power (approximated by a first-order Taylor expansion around the dc value) as a function of base current and temperature-rise phasors as

$$\tilde{p}_{k,{\rm ss}} = \hat{V}_{\rm CC}(\beta_{\rm Q}\tilde{i}_{{\rm B}k,{\rm ss}} + m_\beta I_{\rm BQ}\Delta\tilde{T}_{k,{\rm ss}}) \tag{18}$$

where $\hat{V}_{\rm CC} = V_{\rm CC} - 2(R_{\rm C} + R_{\rm E})\beta_{\rm Q} I_{\rm BQ}$. The relationship between the base-current variation entering each finger is given by

$$\tilde{i}_{{\rm B1,ss}} = -\frac{m_{\rm v}\Delta\tilde{T}_{1,{\rm ss}}}{2R_S} + \frac{m_{\rm v}\Delta\tilde{T}_{2,{\rm ss}}}{2R_S} + \frac{1}{2}\tilde{i}_{{\rm Bt,ss}} \tag{19}$$

$$\tilde{i}_{{\rm B2,ss}} = +\frac{m_{\rm v}\Delta\tilde{T}_{1,{\rm ss}}}{2R_S} - \frac{m_{\rm v}\Delta\tilde{T}_{2,{\rm ss}}}{2R_S} + \frac{1}{2}\tilde{i}_{{\rm Bt,ss}} \tag{20}$$

where $\tilde{i}_{{\rm Bt,ss}} = \tilde{i}_{{\rm B1,ss}} + \tilde{i}_{{\rm B2,ss}}$ is the total base-current variation entering the device. The temperature-rise phasors are calculated as

$$\Delta\tilde{\boldsymbol{T}}_{\rm ss} = \tilde{\mathbf{Z}}_{\rm th}\tilde{\boldsymbol{p}}_{\rm ss} \tag{21}$$

where $\Delta\tilde{\boldsymbol{T}}_{\rm ss} = [\Delta\tilde{T}_{1,{\rm ss}}, \Delta\tilde{T}_{2,{\rm ss}}]^{\rm T}$, $\tilde{\boldsymbol{p}}_{\rm ss} = [\tilde{p}_{1,{\rm ss}}, \tilde{p}_{2,{\rm ss}}]^{\rm T}$, and $\tilde{\mathbf{Z}}_{\rm th}$ is the thermal impedance matrix associated with (15).

Using (18) –(21), the temperature rise in each finger is easily shown to be the solution of the linear system

$$\mathbf{J}\Delta\tilde{\boldsymbol{T}} = \frac{1}{2}\tilde{\mathbf{Z}}_{\rm th}\begin{bmatrix}1\\1\end{bmatrix}\tilde{i}_{{\rm Bt,ss}} \tag{22}$$

where $\mathbf{J}$ is defined in (23), shown at the top of the following page, with $\tilde{Z}_{{\rm th},S}$ and $\tilde{Z}_{{\rm th,C}}$ being the diagonal and off-diagonal elements of $\tilde{\mathbf{Z}}_{\rm th}$, respectively, In (23), the following parameters have been exploited:

$$\alpha = \hat{V}_{\rm CC} m_\beta I_{\rm BQ} \quad \delta = \frac{\hat{V}_{\rm CC}\beta_{\rm Q} m_{\rm V}}{2R_S}. \tag{24}$$

Due to the decreasing behavior of the current gain (β) and the diode turn-on voltage ($v_{\rm BE}$ for a constant $i_{\rm B}$), the parameters

$$\mathbf{J} = \begin{bmatrix} 1-\alpha\tilde{Z}_{\mathrm{th},S}+\delta(\tilde{Z}_{\mathrm{th},S}-\tilde{Z}_{\mathrm{th,C}}) & -\delta(\tilde{Z}_{\mathrm{th},S}-\tilde{Z}_{\mathrm{th,C}})-\alpha\tilde{Z}_{\mathrm{th,C}} \\ -\delta(\tilde{Z}_{\mathrm{th},S}-\tilde{Z}_{\mathrm{th,C}})-\alpha\tilde{Z}_{\mathrm{th,C}} & 1-\alpha\tilde{Z}_{\mathrm{th},S}+\delta(\tilde{Z}_{\mathrm{th},S}-\tilde{Z}_{\mathrm{th,C}}) \end{bmatrix} \tag{23}$$

δ and α, which are dimensionally equivalent to a conductance, are always negative.

For autonomous oscillations to be allowed for, system (22) should admit a nontrivial solution for $\tilde{i}_{\mathrm{Bt,ss}} = 0$, and therefore, **J** should be singular. Since **J** is symmetric, the singularity condition reduces to $J_{11} = \pm J_{12}$, thus identifying odd $(+)$ and even $(-)$ oscillation modes into the circuit.

For the odd mode $(\Delta\tilde{T}_{\mathrm{ss},1} = -\Delta\tilde{T}_{\mathrm{ss},2})$, the oscillation condition is satisfied when

$$\mathrm{Im}\{\tilde{Z}_{\mathrm{th},S}-\tilde{Z}_{\mathrm{th,C}}\}=0 \tag{25a}$$
$$(2\delta-\alpha)\mathrm{Re}\{\tilde{Z}_{\mathrm{th},S}-\tilde{Z}_{\mathrm{th,C}}\}=-1 \tag{25b}$$

while for the even mode $(\Delta\tilde{T}_{\mathrm{ss},1} = \Delta\tilde{T}_{\mathrm{ss},2})$, it takes the form

$$\mathrm{Im}\{\tilde{Z}_{\mathrm{th},S}-\tilde{Z}_{\mathrm{th,C}}\}=0 \tag{26a}$$
$$\alpha\mathrm{Re}\{\tilde{Z}_{\mathrm{th},S}-\tilde{Z}_{\mathrm{th,C}}\}=1. \tag{26b}$$

Both oscillation modes lead to the same condition on the imaginary part of $\tilde{Z}_{\mathrm{th},S}-\tilde{Z}_{\mathrm{th,C}}$, yielding an analytical expression for the spurious oscillation frequency, which results to be dependent only on the thermal network parameters

$$f_{\mathrm{osc}} = \frac{1}{2\pi}\sqrt{\frac{C_{\mathrm{th},S}R_{\mathrm{th},S}^2 - C_{\mathrm{th,C}}R_{\mathrm{th,C}}^2}{C_{\mathrm{th},S}C_{\mathrm{th,C}}R_{\mathrm{th},S}^2R_{\mathrm{th,C}}^2(C_{\mathrm{th},S}-C_{\mathrm{th,C}})}}. \tag{27}$$

Such oscillation frequency corresponds to the one predicted by the full numerical model at the bifurcation onset. On the other hand, the conditions on the real part of $\tilde{Z}_{\mathrm{th},S}-\tilde{Z}_{\mathrm{th,C}}$ allows one to identify the bifurcation onset as a function of electrical parameters, e.g., I_{BQ} and V_{CC}, which set the value of the dc working point. As far as the even mode is concerned, the second condition in (26) would require that, at the oscillation frequency, $\mathrm{Re}\{Z_{\mathrm{th}11}-Z_{\mathrm{th}12}\} < 0$, i.e., a thermal coupling effect that is larger than the self-term one, which is not realizable from a physical standpoint. Thus, the circuit may support only odd oscillation modes, provided that conditions (25) hold. This may be further verified by evaluating the input admittance seen at the base-current generator, which results to be nonzero for every biasing condition and frequency, thus indicating that the circuit does not admit for even (common)-mode oscillations.

Starting from (25b) calculated at $f = f_{\mathrm{osc}}$, some algebraic manipulations allow one to obtain the condition for the instability onset

$$2\delta-\alpha = \frac{R_{\mathrm{th},S}C_{\mathrm{th},S}+R_{\mathrm{th,C}}C_{\mathrm{th,C}}}{R_{\mathrm{th},S}R_{\mathrm{th,C}}(C_{\mathrm{th},S}-C_{\mathrm{th,C}})} = g_{\mathrm{NS}}. \tag{28}$$

Finally, by substituting δ and α from (24), we derived a closed-form expression for the bifurcation curve in the $(V_{\mathrm{CC}}, I_{\mathrm{C}}(I_{\mathrm{BQ}}))$ plane separating the stable (left of the curve) and unstable (right) device operation regions

$$V_{\mathrm{CC,cr}} = \frac{g_{\mathrm{NS}}}{\frac{\beta_{\mathrm{Q}}m_{\mathrm{VT}}}{R_S}-m_\beta I_{\mathrm{BQ}}} + 2(R_{\mathrm{C}}+R_{\mathrm{E}})\beta_{\mathrm{Q}}I_{\mathrm{BQ}}. \tag{29}$$

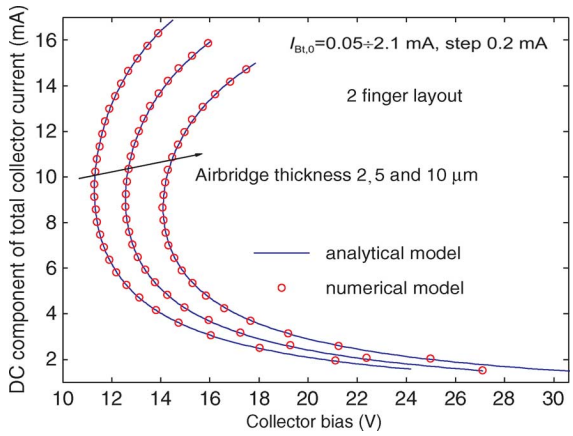

Fig. 9. Comparison between the bifurcation curves computed from the small-signal analytical model and the curves calculated from the full numerical model at different air-bridge thicknesses.

Fig. 9 compares the Neimark–Sacker bifurcation curve calculated according to (29) against the results calculated from the full numerical model. The analytical small-signal model describes with high accuracy the dependence of the bifurcation onset either on the biasing conditions $(V_{\mathrm{CC}}, I_{\mathrm{Bt},0})$ or on the device thermal layout (air-bridge thickness).

IV. Conclusion

An analysis of electrothermal instabilities and oscillations in multifinger HBTs has been presented on the basis of a CAD-oriented harmonic-balance-based frequency domain implementation of the Floquet multiplier evaluation. Other than pointing out several dynamical instability patterns, with their correlation to the behavior of the Floquet multipliers, we have provided a physical circuit-based interpretation of thermal oscillations, with closed-form expressions for the oscillation frequency and oscillation onset condition for the two-finger case.

References

[1] R. H. Winkler, "Thermal properties of high-power transistors," *IEEE Trans. Electron Devices*, vol. ED-14, no. 5, pp. 260–263, May 1967.

[2] N. Rinaldi and V. D'Alessandro, "Theory of electrothermal behavior of bipolar transistors: Part II—Two-finger devices," *IEEE Trans. Electron Devices*, vol. 52, no. 9, pp. 2022–2033, Sep. 2005.

[3] W. Liu, S. Nelson, D. G. Hill, and A. Khatibzadeh, "Current gain collapse in microwave multifinger heterojunction bipolar transistors operated at very high power densities," *IEEE Trans. Electron Devices*, vol. 40, no. 11, pp. 1917–1927, Nov. 1993.

[4] C.-H. Liao, C.-P. Lee, N. L. Wang, and B. Lin, "Optimum design for a thermally stable multifinger power transistor," *IEEE Trans. Electron Devices*, vol. 49, no. 5, pp. 902–908, May 2002.

[5] A. Suárez and R. Quéré, *Stability Analysis of Nonlinear Microwave Circuits*. Norwood, MA: Artech House, 2003.

[6] F. L. Traversa, F. Bonani, and S. Donati Guerrieri, "A frequency-domain approach to the analysis of stability and bifurcations in nonlinear systems described by differential–algebraic equations," *Int. J. Circuit Theory Appl.*, vol. 36, no. 4, pp. 421–439, Jun. 2008.

[7] F. Cappelluti, F. L. Traversa, F. Bonani, and G. Ghione, "A novel, rigorous approach to the dynamic, large-signal stability analysis of semiconductor devices and circuits under electro-thermal interaction," in *IEDM Tech. Dig.*, San Francisco, CA, Dec. 15–17, 2008, pp. 689–692.
[8] F. L. Traversa, F. Cappelluti, F. Bonani, and G. Ghione, "HB-based CAD-oriented dynamic stability analysis of circuits and devices: Application to the assessment of thermal instabilities in multifinger HBTs," in *IEEE MTT-S Int. Microw. Symp. Dig.*, Boston, MA, Jun. 7–12, 2009, pp. 1493–1496.
[9] A. Demir, "Floquet theory and nonlinear perturbation analysis for oscillators with differential–algebraic equations," *Int. J. Circuits Theory Appl.*, vol. 28, no. 2, pp. 163–185, 2000.
[10] L. O. Chua, C. A. Desoer, and E. S. Kuh, *Linear and Nonlinear Circuits*. New York: McGraw-Hill, 1987.
[11] M. Farkas, *Periodic Motions*. New York: Springer-Verlag, 1994.
[12] K. S. Kundert, A. Sangiovanni-Vincentelli, and J. K. White, *Steady-State Methods for Simulating Analog and Microwave Circuits*. Boston, MA: Kluwer, 1990.
[13] F. Cappelluti, F. Bonani, S. Donati Guerrieri, G. Ghione, M. Peroni, A. Cetronio, and R. Graffitti, "A new dynamic, self-consistent electro-thermal model of power HBTs and a novel interpretation of thermal collapse loci in multi-finger devices," in *Proc. Custom Integr. Circuits Conf.*, San Diego, CA, May 6–9, 2001, pp. 397–400.
[14] K. Lu and C. M. Snowden, "Analysis of thermal instability in multifinger power AlGaAs/GaAs HBT's," *IEEE Trans. Electron Devices*, vol. 43, no. 11, pp. 1799–1805, Nov. 1996.
[15] F. L. Traversa, F. Cappelluti, and F. Bonani, "A critical discussion of the current collapse in multifinger HBTs based on Floquet stability analysis," in *Proc. INMMiC*, Malaga, Spain, Nov. 24–25, 2008, pp. 21–24.
[16] B. Bayraktaroglu, J. Barrette, L. Kehias, C. I. Huang, R. Fitch, R. Neidhard, and R. Scherer, "Very high-power-density CW operation of GaAs/AlGaAs microwave heterojunction bipolar transistors," *IEEE Electron Device Lett.*, vol. 14, no. 10, pp. 493–495, Oct. 1993.
[17] D. D'Amore and P. Maffezzoni, "Electro-thermal analysis of paralleled bipolar devices," *Microelectron. J.*, vol. 31, no. 9/10, pp. 753–758, Oct. 2000.
[18] R. S. Burton and P. Dai, "Characterization and modeling of InGaP HBT low-frequency oscillations," *IEEE Trans. Electron Devices*, vol. ED-51, no. 6, pp. 1033–1036, Jun. 2004.

Fabio Lorenzo Traversa was born in Bari, Italy, in 1979. He received the Laurea degree in nuclear engineering and Ph.D. degree in physics from the Politecnico di Torino, Turin, Italy, in 2004 and 2008, respectively.

In 2008, he was a Research Fellow with the Dipartimento di Elettronica, Politecnico di Torino, and since 2009, he has been a Postdoctoral Researcher with the Departament d'Enginyeria Electrònica, Universitat Autònoma de Barcelona, Barcelona, Spain. His research interests are mainly devoted to the physics-based simulation of transport in nanodevices, with special emphasis on the analysis and simulation of quantum correlations. Furthermore, he is also interested in the stability analysis of nonlinear circuits and systems and in the noise analysis of nonlinear circuits.

Federica Cappelluti (S'02–M'03) was born in Ortona, Italy, in 1973. She received the Laurea degree in electronic engineering and Ph.D. degree in electronic and communications engineering from the Politecnico di Torino, Turin, Italy, in 1998 and 2002, respectively.

She is currently an Assistant Professor with the Dipartimento di Elettronica, Politecnico di Torino. Her main research interests concern the system-level and physics-based modeling and simulation of microwave and optoelectronic devices.

Fabrizio Bonani (S'89–M'91–SM'02) was born in Turin, Italy, in 1967. He received the Laurea (*cum laude*) and Ph.D. degrees in electronic engineering from the Politecnico di Torino, Turin, Italy, in 1992 and 1996, respectively.

From October 1994 to June 1995, he was with the ULSI Technology Research Department, Bell Laboratories, Murray Hill, NJ, as a Consultant, working on physics-based noise modeling of electron devices. From August to October 2008, he was a Visiting Scientist with the Ferdinand-Braun-Institut für Höchstfrequenztechnik, Berlin, Germany, where he developed compact noise models for linear and nonlinear applications. Since 1995, he has been with the Dipartimento di Elettronica, Politecnico di Torino, where he is currently an Associate Professor of electronics. His research interests are mainly devoted to the physics-based simulation of semicondutor devices, with special emphasis on the noise analysis of microwave field-effect and bipolar transistors, and to the thermal analysis of power microwave circuits. Furthermore, he is also interested in the stability analysis of nonlinear circuits and systems and in the noise analysis of nonlinear circuits.

Giovanni Ghione (M'87–SM'94–F'07) was born in Alessandria, Italy, in 1956. He received the Electronic Engineering degree (*cum laude*) from the Politecnico di Torino, Turin, Italy, in 1981.

In 1983, he became a Research Assistant with the Politecnico di Torino, and from 1987 to 1990, he was an Associate Professor with the Politecnico di Milano. In 1990, he joined the University of Catania, Catania, Italy, as a Full Professor of electronics, and since 1991, he has been a Full Professor of electronics with the II Faculty of Engineering, Politecnico di Torino, where he is also with the Dipartimento di Elettronica. Since 1981, he has been engaged in Italian and European research projects (ESPRIT 255, COSMIC, and MANPOWER) in the field of active and passive microwave computer-aided design. His current research interests concern the physics-based simulation of active microwave and optoelectronic devices, with particular attention to noise modeling, thermal modeling, and active device optimization. His research interests also include several topics in computational electromagnetics, including coplanar component analysis. He has authored or coauthored over 150 papers and book chapters in the aforementioned fields.

Prof. Ghione is a member of the Editorial Board of the IEEE TRANSACTIONS ON MICROWAVE THEORY AND TECHNIQUES. He is a member of the Associazione Elettrotecnica Italiana.